Dynamics of a colloidal particle driven by continuous time-delayed feedback

Miranda C. R. Bell-Davies,[1,2] Arran Curran,[1,2] Yanyan Liu,[1] and Roel P. A. Dullens[1,2]
[1]*Department of Chemistry, Physical and Theoretical Chemistry Laboratory, University of Oxford, South Parks Road, Oxford OX1 3QZ, United Kingdom*
[2]*Institute for Molecules and Materials, Radboud University, Heyendaalseweg 135, 6525 AJ Nijmegen, The Netherlands*

(Received 17 February 2023; accepted 25 April 2023; published 6 June 2023)

We perform feedback experiments and simulations in which a colloidal dumbbell particle, acting as a particle on a ring, is followed by a repulsive optical trap controlled by a continuous-time-delayed feedback protocol. The dynamics are described by a persistent random walk similarly to that of an active Brownian particle, with a transition from predominantly diffusive to driven behavior at a critical delay time. We model the dynamics in the short and long delay regimes using stochastic delay differential equations and derive a condition for stable driven motion. We study the stochastic thermodynamic properties of the system, finding that the maximum work done by the trap coincides with a local minimum in the mutual information between the trap and the particle position at the onset of stable driven dynamics.

DOI: 10.1103/PhysRevE.107.064601

I. INTRODUCTION

Maxwell's demon uses information to create a temperature gradient in a heat bath without performing any work, seemingly violating the second law of thermodynamics [1]. This paradox was resolved by the realization that there is an entropy change associated with the processes of acquiring information [2], leading to the birth of information thermodynamics [3]. In any experimental realization of Maxwell's demon, there is always a time delay among taking a measurement, performing information processing, and then implementing the feedback, often to the detriment of the feedback engine's efficiency [4]. However, time delays can also be beneficial, for example in the use of delayed feedback to stabilize chaotic motion in engineering applications [5].

When delayed feedback is applied continuously, the system is described by a stochastic delay differential equation (SDDE); a general class of equations which describe any system whose evolution depends on its state some delay time in the past. There are many examples of time-delayed systems across the scientific disciplines [6], including biological motors [7–9], communication and neurological networks [10,11], and even financial markets [12]. Depending on the method by which the delayed feedback is implemented, time delays can either stabilize [13,14] or amplify chaotic motion [15], produce stochastic resonances [16], or display other types of complex dynamics [17,18].

Colloidal particles are often seen as the paradigmatic feedback engine due to the ease of obtaining single-particle information and applying feedback via optical traps after a short-time delay relative to the particle's motion. Colloidal feedback experiments have successfully demonstrated the possibility of information to work conversion with very high efficiency [19–21] or power [22–24], investigated the effect of delay time [4] and measurement error [25], and provided experimental confirmation of several important theoretical findings in information thermodynamics [26,27]. These experiments all apply feedback in discrete steps. Continuous-time-delayed feedback experiments are less common [23], despite simulations predicting many interesting uses. These include enhancing or reversing transport in washboard potentials [28,29], suppressing diffusion using attractive harmonic traps [30], and forming traveling bands of driven colloids using repulsive Gaussian traps [31]. Recently, Kopp *et al.* [32] showed in simulations that a single-particle interacting with a repulsive Gaussian trap controlled via the same feedback protocol as Ref. [31] also displays driven motion similar to the persistent random walk of an active Brownian particle.

Here we create an experimental realization of a single particle on a ring interacting with a repulsive optical trap. We observe a transition from diffusive to driven dynamics with increasing time delay similar to the results of Refs. [31,32]. We characterize the dynamics across this transition and describe the diffusive and driven regimes using the framework of stochastic delay differential equations. We then analyze the work done on the particle and the mutual information between the particle's position at time t and $t - \tau$ in light of the diffusive to driven transition.

II. EXPERIMENTAL METHODS AND THEORETICAL BACKGROUND

A. Experimental setup

The experiments were performed using the optical trapping and microscopy setup described in Ref. [33]. The sample is

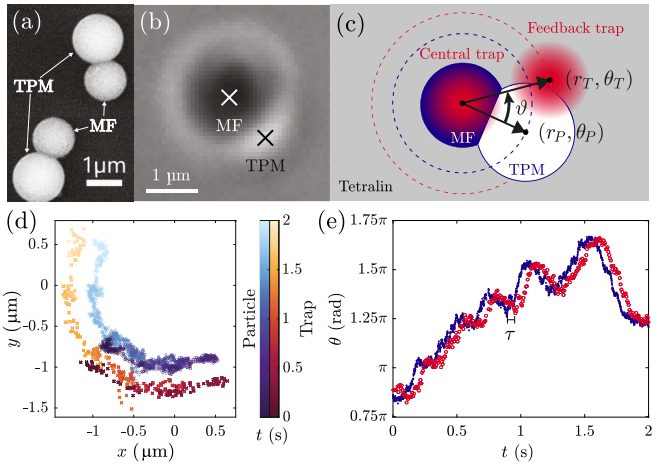

FIG. 1. (a) SEM image of two dumbbell particles. (b) Example image from the experiments. (c) Diagram of the experiment, showing the MF and TPM lobes (blue and white, respectively) and the two optical traps (red). Arrows show the coordinates of the feedback trap and TPM lobe relative to the central trap. (d) Example 2-s trajectory of the TPM lobe (blue) and feedback trap (red). (e) Angular components of the same trajectory.

illuminated from above and a bright-field image is recorded with a CMOS camera. The infrared laser is controlled using a spatial light modulator, which we use to create two optical traps which trap the particle from below. The particle is an optically anisotropic dumbbell-shaped particle which acts as a particle on a ring when placed in an optical trap. Figure 1(a) shows a scanning electron microscopy (SEM) image of the dumbbell particles. The smaller lobe is made of melamine formaldehyde (MF), while the larger lobe is 3-trimethoxysilyl-propylmethacrylate (TPM). They have refractive indices of 1.68 and 1.51. respectively. When placed in tetralin, which has a refractive index of 1.54, the MF lobe has a positive refractive index mismatch so experiences an attractive potential from optical traps, while the TPM lobe has a negative refractive index mismatch so feels a repulsive potential. Placing the particle in a single, stationary optical trap causes the MF lobe to be trapped while the TPM lobe rotates around it at a radius of $r_P = 1.23\ \mu$m. Figure 1(b) shows an example image from one of the experiments. The dark spot surrounded by a light ring is the MF lobe and the light spot with a dark ring is the TPM lobe. The TPM lobe is tracked in real time at 1000 fps by thresholding the image and calculating its center of mass. After tracking the TPM lobe for a delay time τ, an additional feedback-controlled trap is switched on and moved to the particle's position one delay time ago, following the feedback protocol

$$r_T(t) = 1.3 r_P(t-\tau),\ \theta_T(t) = \theta_P(t-\tau). \tag{1}$$

The feedback trap's position is then updated at a rate of 156 Hz. Figure 1(c) shows a diagram of the experimental setup. The MF lobe is far away enough from the feedback trap that they do not interact, but the TPM lobe is repelled and attempts to move away from the trap around the ring. Figures 1(d) and 1(e) illustrate the feedback protocol with an example trajectory, showing the feedback trap moving around a larger radius than the particle and following its position in θ after a delay time τ.

B. Equation of motion

From this point onwards we ignore the central trap and MF lobe and treat the TPM lobe as a particle confined to a ring of fixed radius r_P. The particle's angular position, θ_P, evolves according to the following one-dimensional (1D) Langevin equation:

$$r_P \frac{d\theta_P}{dt} = \frac{1}{\zeta} F(\theta_P, \theta_T) + \xi(t), \tag{2}$$

where ζ is the drag constant of the particle, F is the force from the trap, and $\xi(t)$ is Gaussian white noise with $\langle \xi(t) \rangle = 0$, $\langle \xi(t)\xi(t') \rangle = 2(k_B T/\zeta)\delta(t-t')$. The optical trap exerts a repulsive Gaussian potential on the particle with a stiffness k and depth V_0. It is convenient to define the following constants:

$$\zeta_{\text{rad}} = r_P^2 \zeta, \tag{3}$$

$$K = \frac{k}{\zeta_{\text{rad}}} r_T r_P \exp\left[-\frac{k(r_P - r_T)^2}{2V_0}\right], \tag{4}$$

$$\phi = \sqrt{\frac{V_0}{k r_P r_T}}. \tag{5}$$

Here ζ_{rad} is the angular drag constant, ϕ is the trap width in radians, and K is a frequency proportional to the trap stiffness. K is a repulsive, angular equivalent of the corner frequency of a trap, which defines the frequency at which the particle explores the trap width [34]. These constants allow the trap force to be written as:

$$F(\vartheta) = \zeta_{\text{rad}} K \sin\vartheta \exp\left(\frac{1-\cos\vartheta}{\phi^2}\right). \tag{6}$$

where $\vartheta(t) = \theta_P(t) - \theta_P(t-\tau)$ is the angular distance between the particle and the trap [shown in Fig. 1(b)] and the force has units of kg rad s^{-2}. When the trap width is small compared to the radius around which the particle moves ($\phi \ll r_P$), applying the small-angle approximation reduces Eq. (6) to the following Gaussian force:

$$F(\vartheta) \approx \zeta_{\text{rad}} K \vartheta \exp\left(-\frac{\vartheta^2}{2\phi^2}\right). \tag{7}$$

Note that ϑ must always be within $[-\pi, \pi]$ as this expression is not periodic. The trap force is maximized when $\vartheta = \phi$. At this angle, the trap pushes the particle at a velocity of $v_m = e^{-1/2} K\phi$. Another important constant is $\tau_m = \phi/v_m = e^{1/2}K^{-1}$, the time taken for the particle to move a distance equal to the trap width at the maximum velocity.

Finally, rewriting Eq. (2) with the angular drag constant, ζ_{rad}, gives the following equation of motion:

$$\frac{d\theta_P}{dt} = \zeta_{\text{rad}}^{-1} F(\vartheta) + \xi_{\text{rad}}(t). \tag{8}$$

Each term in this expression has units of rad s^{-1}. The angular noise term, ξ_{rad}, has a correlation function of $\langle \xi_{\text{rad}}(t)\xi_{\text{rad}}(t') \rangle = (2k_B T/\zeta_{\text{rad}})\delta(t-t')$. From now on, we only use terms in units of radians unless stated otherwise and drop the rad subscript on ξ_{rad} and ζ_{rad}.

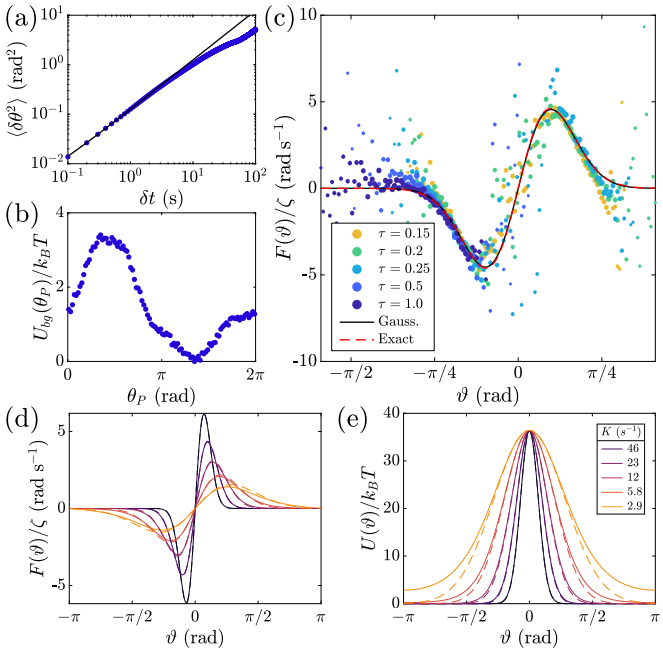

FIG. 2. (a) Angular MSD with linear fit. (b) Background potential around the ring. (c) Trap force measured from the feedback experiments with $\tau = 0.15$ s (yellow) to 1 s (blue), with fits to Eqs. (6) and (7). (d) Exact trap force used in the simulations [Equation (6), solid lines] and the corresponding Gaussian approximations [Equation (7), dashed lines]. The trap depth, V_0, is fixed at the experimentally measured value and the corner frequency is $K_{\text{exp}} \times 2^{1,\ 0,\ -1,\ -2\ \&\ -3}$ (blue to yellow). Consequently, the trap width is $\phi_{\text{exp}} \times 2^{-1/2,\ 0,\ 1/2,\ -1\ \&\ -3/2}$. The purple line with $K = 23$ is the same as the experimentally measured trap force in (d). (e) Corresponding trap potential.

C. Calibration experiments

The experimental trap force, drag constant, and background potential are calibrated using two different experiments. We measure the particle's angular drag constant of $\zeta = 6.64 \times 10^{-8}$ kg μ m^2 s^{-1} from its mean-squared displacement (MSD) in the absence of the feedback trap, shown in Fig. 2(a). From this experiment, we also measure a small background potential around the ring, shown in Fig. 2(b), which biases the particle towards angles of $\theta_P \approx (3/2)\pi$. This background potential has a depth of $3.5k_BT$, an order of magnitude smaller than the potential of the feedback trap.

The force acting on the particle from the feedback trap, which is the same in all experiments, was calibrated *in situ* from the feedback experiments with large delay times using the method of Juniper *et al.* [35]. The measured force, shown in Fig. 2(c), agrees well with the Gaussian form of Eqs. (6) and (7).

D. Simulations

To complement the experiments and further explore the parameter space, we also carry out one-dimensional Brownian dynamics simulations based on the angular Langevin equation [Eq. (8)]. The simulations use the experimentally determined values for the drag constant and trap depth and several different corner frequencies (proportional to the trap stiffness). The trap forces and corresponding potentials used in the simulations are shown in Figs. 2(d) and 2(e).

III. RESULTS AND DISCUSSION

In this section, we characterize the dynamics of the feedback experiments and simulations at different delay times and use SDDEs to describe the system's behavior in the short- and long-delay-time regimes. We then characterize the stochastic thermodynamic properties of the system.

A. Dynamics

First, we characterize the dynamics of the particle at different delay times. Figure 3(a) shows typical trajectories from four representative experiments with delay times of τ =0.01, 0.05, 0.1, and 0.5 s. Note that the effect of the periodic boundary conditions has been removed by constraining the change in angle from one frame to the next to $|\Delta\theta| < \pi$ and therefore allowing θ to have any value. The corresponding MSDs are shown in Fig. 3(b), while Fig. 3(c) shows histograms of the angle between the particle and the trap, $\vartheta = \theta_P(t) - \theta_T(t) = \theta_P(t) - \theta_P(t-\tau)$. As the lag time increases, the trajectories, MSDs, and ϑ distributions all show a dramatic change in behavior. We will now describe each lag time separately.

When $\tau = 0.01$ s, the trajectory appears to be trapped at around 1.5π due to the background potential. The MSD is diffusive ($\propto t^1$) at short times but subdiffusive at long times as a result of the background potential. The short-time diffusion coefficient is slightly larger than the free-diffusion measurement because the trap pushes the particle upwards away from the bottom of the sample cell, decreasing its drag constant. The histogram of the angle between the particle and the trap, $P(\vartheta)$, shown in Fig. 3(c), is a narrow Gaussian centered around 0, consistent with diffusive short-time behavior. The dotted line at the top of Fig. 3(c) shows the trap force profile, showing that the particle spends most of the time near the trap center, where the force is small. This explains why the trajectory is diffusive—the feedback trap always applies a small force to the particle, so has a minimal effect on its diffusive trajectory.

When $\tau = 0.05$ s, the particle's trajectory appears more diffusive, albeit with a slight preference for values of $(1.5 + 2n)\pi$ as a result of the background potential. The mean squared displacement is diffusive at short and long times with a transient superdiffusive ($\propto t^2$) section in between. This t^2 scaling implies driven motion. The histogram of the angle between the particle and the trap, $P(\vartheta)$, is broader and has less Gaussian character. As the particle diffuses further from the trap center, it is then pushed even further by the repulsive trap force, which causes both the non-Gaussian $P(\vartheta)$ and the transient driven behavior in the MSD. This force is sufficient to overcome the background potential, resulting in long-time diffusive motion.

When $\tau = 0.1$ s, the particle moves at a constant velocity over a sustained period before randomly switching direction, resulting in a persistent random walk. This manifests as an MSD which is diffusive at short times, superdiffusive over a large intermediate time range, and diffusive at long times. The

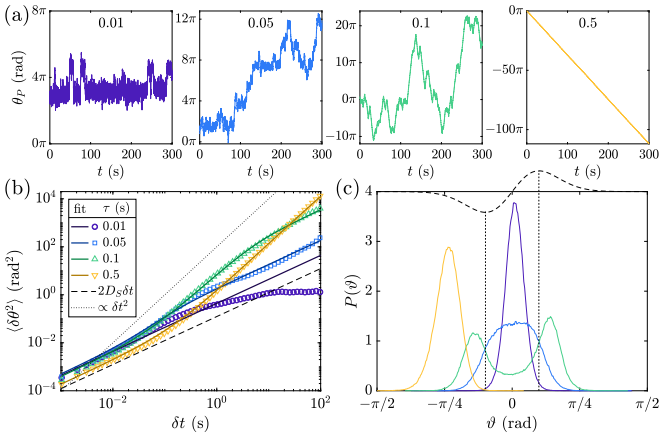

FIG. 3. (a) Particle positions, θ_P, from the first 300 s of experiments with $\tau = 0.01$ s (purple), 0.05 s (blue), 0.1 s (green), and 0.5 s (yellow). (b) MSDs (symbols) with fits to Eq. (9) (lines). The dashed line shows $\langle\delta\theta^2\rangle = 2D_S\delta t$ and the dotted line shows $\langle\delta\theta^2\rangle \propto \delta t^2$. (c) Histogram of the angle between the particle and the trap, $\vartheta = \theta_P - \theta_T$. The dashed line shows $F(\vartheta)$ on an arbitrary vertical axis.

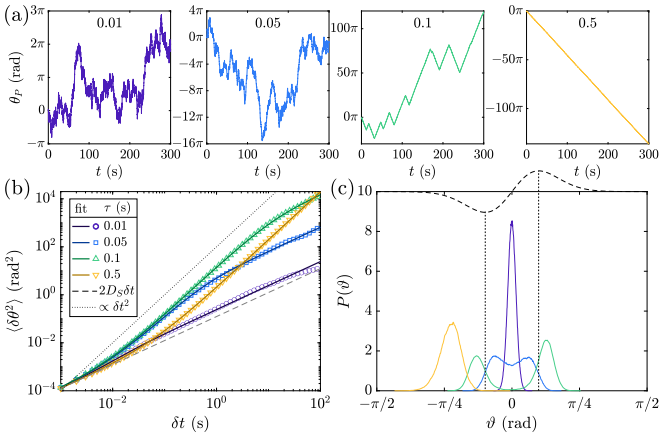

FIG. 4. (a) Particle positions, (b) MSDs with fits to Eq. (9), and (c) histogram of the angle between the particle and the trap for simulations equivalent to the experiments in Fig. 3. All lines and symbols have the same meaning as in Fig. 3.

long-time diffusive section is a result of the random direction changes and has a significantly larger diffusion coefficient than at short times. $P(\vartheta)$ has two sharp peaks near the position of maximum force. The sharpness of the peaks is consistent with the uniformity of the velocity in the driven segments of the trajectory.

At the largest delay time of 0.5 s, the particle moves at a constant velocity without switching direction over the whole experiment. The MSD switches from diffusive at short times to driven at long times. The $P(\vartheta)$ distribution shows that this is because the particle is always far from the trap center, so there is a large energy barrier to switching direction. The driven section has a lower velocity than at $\tau = 0.1$ s, reflecting the large average $|\vartheta|$.

The same trends can be seen more clearly in the simulations in Fig. 4, where there are no effects from the background potential, out-of-plane motion, or tracking errors. This confirms our interpretation of the experimental results. The MSDs in Fig. 4(b) show that the simulations all have the same diffusion coefficient at short times. At intermediate times, the trajectories all have a transient driven, superdiffusive section. For long delay times, this corresponds to motion at a constant speed, as shown in Fig. 4(a). As the delay time increases, the driven section last for longer as the particle hops from one side of the trap to the other less frequently. This is a result of its larger distance from the trap center, as shown in Fig. 4(c). Diffusive motion is recovered at long times for all but the largest delay time.

Overall, except for the subdiffusive long-time behavior of the experiment with $\tau = 0.01$ s due to the background potential, the experiments and simulations can all be described by short-time diffusive motion characterized by the short-time diffusion coefficient, D_S, combined with driven motion at a constant speed, v, and random changes of direction at an average rate of λ. This is exactly the type of motion displayed by a model 1D active Brownian particle, which has an MSD of [36,37]

$$\langle\delta\theta^2\rangle = \left(2D_S + \frac{v^2}{\lambda}\right)t + \frac{v^2}{2\lambda^2}(e^{-2\lambda t} - 1). \tag{9}$$

The limiting values at short and long times are

$$\langle\delta\theta^2\rangle(t \ll \lambda^{-1}) = 2D_S t + v^2 t^2, \tag{10}$$

$$\langle\delta\theta^2\rangle(t \gg \lambda^{-1}) = \left(2D_S + \frac{v^2}{\lambda}\right)t = 2D_L t, \tag{11}$$

where $D_L = D_S + v^2/2\lambda$ is the long-time diffusion coefficient. Each MSD is fitted with Eq. (9) to obtain the driving speed, v, and reorientation rate, λ. The experiments and simulations show good agreement with the fits, which are plotted in Figs. 3(b) and 4(b).

The values of $D_L - D_S$, v, and λ from each fit are shown in Fig. 5. There is good agreement between the experiments and simulations. The long-time diffusion coefficient, D_L [Fig. 5(a)], increases dramatically with increasing delay time until is becomes too large to measure. The speed, v [Fig. 5(b)], initially increases with increasing τ, reaches a maximum value close to v_m when $K\tau \approx 1.5$ and then decreases with increasing τ. The reorientation rate, λ [Fig. 5(c)], decreases rapidly with increasing τ.

B. Stochastic delay differential equations

We now explain the measured trends in v, λ, and D_L using the framework of stochastic delay differential equations. At short delay times, we use two different approaches to predicting the long-time diffusion coefficient. The first approach is based on Guillouzic *et al.* [38], who showed that any delay differential equation can be approximated by a delay-free Langevin equation in the limit of small delay times ($\tau \to 0$). Their method gives the following approximate equation of motion:

$$\frac{d\theta_P}{dt} \approx (1 + K\tau)\xi(t). \tag{12}$$

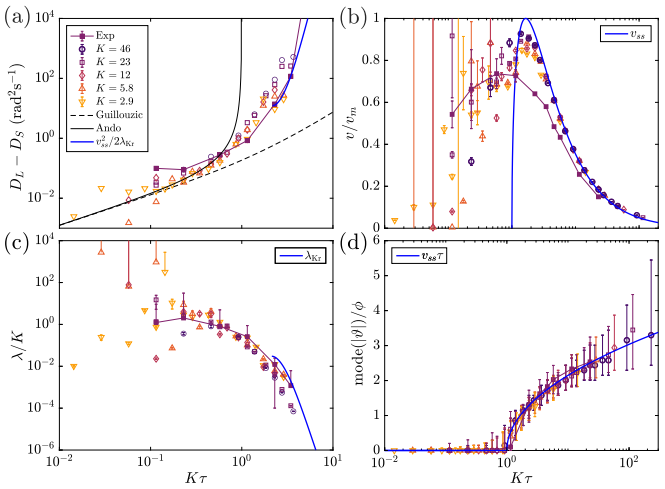

FIG. 5. (a) Long-time diffusion coefficient, D_L, as a function of the delay time, τ, in all experiments (purple filled squares) and simulations (blue to yellow empty symbols). Delay times are scaled by the corner frequency, K. Dashed and solid black lines show Eqs. (13) and (14), respectively, while the blue line shows $D_L - D_S = v_{ss}^2/2\lambda_{Kr}$ from Eqs. (16) and (19). (b) Driving speed, v, in all experiments and simulations [same symbols as (a)], with the steady-state velocity from Eq. (16) (blue line). (c) Reorientation rate, λ [same symbols as (a)], and theoretical rate from Eq. (19) (blue line). (d) Most probable angular distance, $|\vartheta|$ [same symbols as (a)], and the steady-state position, $\vartheta_{ss} = v_{ss}\tau$, from Eq. (16) (blue line).

This predicts purely diffusive motion in the limit of small delay times, with an enhanced diffusion coefficient of

$$D_L = D_S(1 + K\tau)^2, \tag{13}$$

where $D_S = k_B T/\zeta$ is the short-time diffusion coefficient. Figure 5(a) shows that this expression correctly predicts D_L at short delay times but significantly underestimates it at long delay times because it does not include a driven component to the particle's motion.

The second approach is based on Kuchler and Mench's analysis of linear SDDEs [39]. Equation (8) reduces to a linear SDDE in the limit of small ϑ, where the trap is approximately harmonic. Using the results of Ref. [39], Ando *et al.* [30] showed that the long-time diffusion coefficient of a particle in an attractive harmonic trap controlled by our feedback protocol [$\theta_T(t) = \theta_P(t - \tau)$] is given by

$$D_L = \frac{D_S}{(1 - K\tau)^2}. \tag{14}$$

Note that Eqs. (14) and (13) are related via a Taylor expansion. This expression is also valid for a repulsive harmonic trap (with positive rather than negative K) when $\tau < K^{-1}$, where K is the corner frequency of the trap. This timescale defines the transition between diffusive and driven dynamics. In the short delay time limit defined by $\tau < K^{-1}$, Eq. (14) describes the measured increase in D_L with increasing τ slightly better than Eq. 13. Above this point, D_L instead diverges exponentially, with the implication that a diffusive state is not stable. Equation (14) does not predict D_L at long delay times because it does not account for the random reorientations in the driving direction, without which D_L would tend to infinity.

In order to describe the diffusion coefficient in the large τ regime, we start by deriving an expression for the driving speed, v, which we then use to calculate the reorientation rate, λ, and finally combine these two quantities to obtain D_L. We assume that the system settles into a driven nonequilibrium steady state, and consider a deterministic version of the Langevin equation of motion (Eq. 8) with the approximate Gaussian force [Eq. (7)]. If the particle moves at a constant velocity of $dx/dt = v_{ss}$, then the angle between the particle and the trap is fixed at $\vartheta = v_{ss}\tau$. Substituting these into the Langevin equation gives

$$v_{ss} = K v_{ss}\tau \exp\left(-\frac{v_{ss}^2\tau^2}{2\phi^2}\right), \tag{15}$$

and solving for v_{ss} yields the steady-state velocity,

$$v_{ss} = \begin{cases} \pm\frac{\phi}{\tau}\sqrt{2\ln(K\tau)} & \tau \geqslant K^{-1} \\ 0 & \forall\tau \end{cases}. \tag{16}$$

The diffusive state with $v_{ss} = 0$ exists at all delay times, but the two (positive and negative) driven steady states are only possible at long delay times of $\tau > K^{-1}$. This agrees with the short delay time theory in Eq. (14) [30], which also predicts a transition from diffusive to driven motion at $\tau = K^{-1}$.

Figure 5(b) compares the steady-state velocity, v_{ss}, to the measured speed, v, from all experiments and simulations. Scaling the delay time by K^{-1} and the velocities by v_m collapses all experiments and simulations onto the same curve, which reaches the maximum possible value of v_m when $\tau = \tau_m = e^{1/2}K^{-1}$. The measured velocities show good agreement with v_{ss} at long delay times of $K\tau > 1$, confirming that these experiments and simulations are in the driven steady state. Equation (16) also predicts a steady-state angle between the particle and the trap of $\vartheta_{ss} = v_{ss}\tau$. Figure 5(d) shows that this steady-state angle agrees very well with the most probable $|\vartheta|$ taken from the maximum point of a histogram of $|\vartheta|$, once again confirming the validity of Eq. (16).

We will now use the steady-state velocity in Eq. (16) to find an expression for the switching rate, λ. Because the trap moves at a constant angular velocity v_{ss}, the potential energy acting on the particle in the rotating frame of reference, moving with the trap at v_{ss}, is tilted. The effective potential acting on the particle combines the Gaussian trap potential, $U_T(\vartheta)$, with a linear term, $-\zeta v_{ss}\vartheta$, arising from the motion at a constant angular velocity:

$$U_{\text{eff}}(\vartheta) = U_T(\vartheta) - \zeta v_{ss}\vartheta. \tag{17}$$

This potential has a minimum and maximum at

$$\begin{aligned} \vartheta_{\min} &= \pm\phi\sqrt{2\ln(K\tau)}, \\ \vartheta_{\max} &= \pm\phi\sqrt{-W_0\left[\frac{-2\ln(K\tau)}{(K\tau)^2}\right]}, \end{aligned} \tag{18}$$

where $W_0(x)$ is the 0th branch of the Lambert function. Figures 6(a)–6(c) shows the effective potential, $U_{\text{eff}}(\vartheta)$, arising from the three possible steady states (positive, negative, and zero v_{ss}) at different delay times. When $1 < \tau < e^{1/2}$, the steady-state angle between the particle and the trap, $\theta_{ss} = v_{ss}\tau$ [shown with crosses in Fig. 6(a)], corresponds to the local maximum in the tilted potential. Consequently, there is no

energy barrier to the particle moving to the other side of the trap, making the driven state as unstable as the diffusive state with $v_{ss} = 0$. When $K\tau = e^{1/2}$ [Fig. 6(b)], the steady-state position is a saddle point, and when $K\tau > e^{1/2}$ [Fig. 6(c)], θ_{ss} corresponds to a local minimum in the tilted potential. In this case, the trajectory switches direction when the particle hops from one potential minimum to the other over the potential barrier, which happens at a rate λ given by Kramer's escape problem:

$$\lambda_{Kr}^{-1} = \frac{2\pi\zeta}{\sqrt{|U''_{max}U''_{min}|}} \exp\left(\frac{U_{max} - U_{min}}{k_BT}\right). \tag{19}$$

This expression assumes that escape is a Poisson process, which is valid in the limit of $\tau \gg \tau_m$, when the energy barrier is large and the local maximum and minimum are far apart. Equation (19) can therefore be used to calculate the reorientation rate, λ, in the long-delay-time regime. Figure 5(c) compares this theoretical reorientation rate to the measured values from the experiments and simulations. The few measurements of λ in the region in which λ_{Kr} can be calculated agree well with λ_{Kr}.

The steady-state velocity, v_{ss} [Eq. (16)], and the escape rate, λ_{Kr} [Eq. (19)], can now be combined to calculate an expression for the long-time diffusion coefficient of the system, $D_L = D_S + v_{ss}^2/2\lambda_{Kr}$, in the driven regime where $\tau \gg \tau_m$. Figure 5(a) compares this theory to the measured D_L from all experiments and simulations. There is reasonably good agreement, although Kramer's escape equation is only valid for a few data points where D_L can only be measured. This confirms that the dynamics in the long-delay-time regime are well described by a driven steady state with a tilted effective potential.

C. Stochastic thermodynamics

In this section we discuss the stochastic thermodynamics of the feedback process. First, we consider the average rate of work done on the particle by the feedback trap, $\langle \dot{w} \rangle$, shown in Fig. 6(d). This is calculated using Eq. (6) of the supplementary material. At low τ, the simulations have a low $\langle \dot{w} \rangle$ which slowly increases to a maximum at $\tau_m = e^{1/2}/K$. This is because as $P(\vartheta)$ broadens with increasing τ (shown in Figs. 3 and 4), the average $F\dot{x} \propto \zeta F^2$ also increases. The work done by the trap at low τ is significantly larger in the experiments than in the simulations, probably because tracking errors broaden $P(\vartheta)$. When $\tau > K^{-1}$, so the system is in the driven steady state, the rate of work done follows the same shape as the speed, v, peaking at $\tau = \tau_m = e^{1/2}K^{-1}$, where the steady-state velocity is maximized. The inset shows $\langle \dot{w} \rangle$ for the simulations and experiments with $\tau > \tau_m$ as a function of the speed, v. The points all sit very close to the $\langle \dot{w} \rangle = \zeta v^2$ line, which is the minimum power required to drive a particle at a constant speed [40]. This implies that almost all of the work done on the particle is used to drive it at the average speed, making the feedback driving almost as efficient as driving the particle with a constant force.

Another important thermodynamic quantity in a feedback experiment is the mutual information, I, between the particle

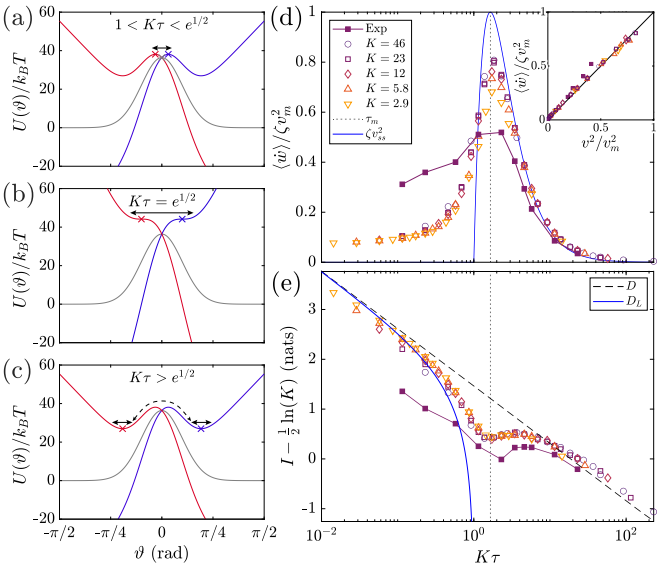

FIG. 6. [(a)–(c)] Effective potential when a particle is driven at the positive (red), negative (blue), and zero (gray) steady-state velocity [Eq. (16)]. Crosses mark the steady-state position and arrows illustrate the region of the potential explored by the particle. (d) Rate of work done relative to the maximum value, $\dot{w}/(\zeta v_m^2)$, against rescaled delay time, $K\tau$, for all experiments and simulations. Inset: Rate of work done, $\dot{w}/\zeta v_m^2$, against the steady-state velocity, v^2/v_m^2. (e) Mutual information between the particle and trap position, I, shifted by $\frac{1}{2}\ln(K)$, against $K\tau$, for all experiments and simulations. The black dashed and solid blue line shows the theoretical value for a freely diffusing particle [see Eq. (15) of the supplementary material] with diffusion coefficients of D_S and $D_L = D_S(1 - K\tau)^{-2}$, respectively. Colors and symbols are the same as in Fig. 5.

position at time t (the system) and $t - \tau$ (the measurement):

$$I = \int_{-\pi}^{\pi} p_m(\vartheta) \ln p_m(\vartheta) d\vartheta + \ln(2\pi), \tag{20}$$

derived in the supplementary material. We use a mirrored probability distribution, $p_m(\vartheta) = [p(\vartheta) + p(-\vartheta)]/2$, to account for the fact that the measured $p(\vartheta)$ from a single finite experiment is not always symmetric, despite the equal probability of the particle being driven to the left or the right. The result is shown in Fig. 6(e) for all experiments and simulations. The mutual information shows interesting nonmonotonic behavior with a local minimum at τ_m, the delay time where the power was maximized.

The inverse relationship between the work and the mutual information can be rationalized by considering the effective potential experienced by the particle, which combines the repulsive trap potential with the tilted effective potential from the steady-state driving velocity. At short delay times of $\tau < \tau_m$, the particle sits on a local maximum of this effective potential, as shown in Fig. 6(a), so the particle diffuses freely. The angle distribution, $p(\vartheta)$, therefore becomes broader with increasing τ, causing the work done on the particle to increases and the mutual information to decrease in line with the theoretical value for free diffusion in Eq. (15) of the supplementary material. When $\tau > \tau_m$, the particle instead sits in a local minimum in the effective potential, as illustrated

in Fig. 6(c). The particle is confined by this effective potential, causing the $p(\vartheta)$ distribution to become more sharply peaked, and so increasing the mutual information. At $\tau = \tau_m$, shown in Fig. 6(b), the particle is driven at the maximum velocity while existing in an unstable state, resulting in a broad $p(\vartheta)$ and hence the local minimum in I. The local minimum in the mutual information between the particle and the trap and the local maximum in the work done on the particle therefore both occur as a result of the system switching from a diffusive steady state to a stable driven steady state.

IV. CONCLUSIONS

We have characterized the dynamics of a particle on a ring interacting with a feedback controlled repulsive optical trap over several orders of magnitude of the delay time, τ. We have shown that at short delay times, the system exists in a diffusive state which is well described by the theory of stochastic delay differential equations. At long delay times, there is a transition to a driven steady state in which the particle and trap move at a constant speed, but randomly switch direction. Unlike in two dimensions, changes in direction can only occur when the particle hops over the trap, leading to a more stable direction of motion. We showed that the driven state exists when there is a nonzero solution to $v_{ss} = F(v_{ss}\tau)$, and that it is stable when $v_{ss}\tau$ is at a local minimum of the tilted effective potential $U_T(\vartheta) - v_{ss}\vartheta$. These results can be applied more generally to determine whether any system described by a stochastic delay differential equation has a stable driven state. We also analyzed the stochastic thermodynamics of the feedback driven system and found that almost all of the work done on the particle is converted into driving it at a constant speed. The maximum power input coincided with the minimum mutual information. We rationalize this relationship by considering the particle's diffusion in the tilted effective potential $U_T(\vartheta) - v_{ss}\vartheta$, showing that the minimum mutual information occurs when the system switches from an unstable to a stable driven steady state.

ACKNOWLEDGMENTS

We thank Andrew Balin for useful discussions. The European Research Council (ERC Consolidator Grant No. 724834 OMCIDC) is acknowledged for financial support.

APPENDIX

1. Work

The stochastic thermodynamic definition of the work done on the particle subject to a force $F(x,t) = -(\partial U/\partial x)_t$ is [41,42]

$$dw = F(x,t)dx + dU. \tag{A1}$$

In order to calculate the work done over a single stochastic trajectory, $w[x(t)]$, which is sampled at a discrete time interval of Δt, we use the Stratanovich interpretation of dx (i.e. the central difference) [3,43]. The rate of work done is therefore calculated using:

$$\dot{w} = F(x_n, t_n)\frac{x_{n+1} - x_{n-1}}{2\Delta t} + U\left(\frac{x_{n+1} + x_n}{2}\right) - U\left(\frac{x_n + x_{n-1}}{2}\right), \tag{A2}$$

where n is the frame number. Note that when a particle is driven at a constant average velocity v with a nonconservative force, such that $dU = 0$, the rate of work done is given by [40]

$$\langle \dot{w} \rangle = \zeta v^2. \tag{A3}$$

Driving with a constant force is the most efficient way to move a particle (in the absence of information) [40].

2. Information

During a feedback process, a measurement device gathers information about the state of the system and uses that information to apply feedback. As the device performs a measurement, its state may change, leading to a change in its entropy. The thermodynamics of the feedback process therefore depends not just on the system and surrounding solvent, but also the measurement device. This is quantified by the mutual information between the state of the system, x, and the state of the measurement device, y [3]. The mutual information is defined as [44]

$$I = \sum_{x,y} p(x,y) \ln\left[\frac{p(x,y)}{p(x)p(y)}\right], \tag{A4}$$

where $p(z)$ is the probability of state z. If x and y are continuous, as in our experiments, then the sum is replaced by the integral

$$I = \iint dxdy\; p(x,y) \ln\left[\frac{p(x,y)}{p(x)p(y)}\right], \tag{A5}$$

where $p(z)$ now represents a probability density function. I is a measure of how narrowly $p(x,y)$ is distributed; it is largest when $p(x,y)$ has a single sharp peak, and smaller when $p(x,y)$ has several broad peaks.

In our feedback experiment, there is a delay time τ between the start and end of the measurement. The state of the system is therefore the particle position at time t, while the state of the measurement device is the particle position at time $t - \tau$, which we set as the trap position at time t. The mutual information is given by

$$I = \int_{-\pi}^{\pi}\int_{-\pi}^{\pi} d\theta_P d\theta_T\, p(\theta_P|\theta_T)p(\theta_T) \ln\left[\frac{p(\theta_P|\theta_T)}{p(\theta_P)}\right], \tag{A6}$$

where we have replaced the joint probability of θ_P and θ_T with the conditional probability of θ_P at a given θ_T using $p(\theta_P, \theta_T) = p(\theta_p|\theta_T)p(\theta_T)$. If we assume that all positions around the ring have the same energy, so are equally probable, then $p(\theta_P) = p(\theta_T) = (2\pi)^{-1}$ for all $\theta_{P/T}$. Furthermore, $p(\theta_P|\theta_T)$ only depends on the angle between the particle and the trap, $\vartheta = \theta_P - \theta_T$, so we can replace $p(\theta_P|\theta_T)$ in Eq. (A6) with $p(\vartheta)$ by integrating over $d\theta_T$. This reduces Eq. (A6) to

$$I = \int_{-\pi}^{\pi} d\vartheta\, p(\vartheta) \ln p(\vartheta) + \ln(2\pi). \tag{A7}$$

In order to illustrate how I depends on the delay time, τ, it is useful to consider the case of free diffusion. In the small τ limit when $4D\tau/\pi^2 \ll 1$, so that particle has not had time to diffuse around the ring, ϑ has the following Gaussian probability distribution:

$$p(\vartheta) = \frac{1}{\sqrt{4\pi D\tau}} \exp\left(\frac{-\vartheta^2}{4D\tau}\right), \tag{A8}$$

which leads to a mutual information of

$$I \approx \frac{1}{2}\left[\ln\left(\frac{\pi}{D}\right) - 1 - \ln(\tau)\right]. \tag{A9}$$

Conversely, in the long τ limit, all positions on the ring become equally likely, so $p(\vartheta) \to (2\pi)^{-1}$ and $I \to 0$ when $\tau \to \infty$. The mutual information therefore decreases linearly with $\ln \tau$ until it reaches a plateau at $I = 0$.

[1] H. S. Leff and A. F. Rex, *Maxwell's Demon 2: Entropy, Classical and Quantum Information, Computing* (Institute of Physics, Bristol, UK, 2003).
[2] L. Szilard, Z. Phys. **53**, 840 (1929).
[3] L. Peliti and S. Pigolotti, *Stochastic Thermodynamics: An Introduction* (Princeton University Press, Princeton, NJ, 2021).
[4] S. Toyabe, T. Sagawa, M. Ueda, E. Muneyuki, and M. Sano, Nat. Phys. **6**, 988 (2010).
[5] Y. N. Kyrychko and S. J. Hogan, J. Vib. Contr. **16**, 943 (2010).
[6] J.-P. Richard, Automatica **39**, 1667 (2003).
[7] Y. Tu, Proc. Natl. Acad. Sci. USA **105**, 11737 (2008).
[8] B. Novák and J. J. Tyson, Nat. Rev. Mol. **9**, 981 (2008).
[9] R. K. Schmitt, J. M. R. Parrondo, H. Linke, and J. Johansson, New J. Phys. **17**, 065011 (2015).
[10] A. Longtin, J. G. Milton, J. E. Bos, and M. C. Mackey, Phys. Rev. A **41**, 6992 (1990).
[11] K. Mergenthaler and R. Engbert, Phys. Rev. Lett. **98**, 138104 (2007).
[12] P. S. Grassia, Eur. Phys. J. B **17**, 347 (2000).
[13] K. Pyragas, Phys. Lett. A **170**, 421 (1992).
[14] P. Hövel and E. Schöll, Phys. Rev. E **72**, 046203 (2005).
[15] T. Albers, D. Müller-Bender, L. Hille, and G. Radons, Phys. Rev. Lett. **128**, 074101 (2022).
[16] S. Kim, S. H. Park, and H.-B. Pyo, Phys. Rev. Lett. **82**, 1620 (1999).
[17] L. S. Tsimring and A. Pikovsky, Phys. Rev. Lett. **87**, 250602 (2001).
[18] T. Albers, D. Müller-Bender, and G. Radons, Phys. Rev. E **105**, 064212 (2022).
[19] G. Paneru, D. Y. Lee, T. Tlusty, and H. K. Pak, Phys. Rev. Lett. **120**, 020601 (2018).
[20] T. Admon, S. Rahav, and Y. Roichman, Phys. Rev. Lett. **121**, 180601 (2018).
[21] M. Ribezzi-Crivellari and F. Ritort, Nat. Phys. **15**, 660 (2019).
[22] D. Y. Lee, J. Um, G. Paneru, and H. K. Pak, Sci. Rep. **8**, 12121 (2018).
[23] B. J. Lopez, N. J. Kuwada, E. M. Craig, B. R. Long, and H. Linke, Phys. Rev. Lett. **101**, 220601 (2008).
[24] G. Paneru, D. Y. Lee, J.-M. Park, J. T. Park, J. D. Noh, and H. K. Pak, Phys. Rev. E **98**, 052119 (2018).
[25] T. K. Saha, J. N. E. Lucero, J. Ehrich, D. A. Sivak, and J. Bechhoefer, Phys. Rev. Lett. **129**, 130601 (2022).
[26] A. Bérut, A. Arakelyan, A. Petrosyan, S. Ciliberto, R. Dillenschneider, and E. Lutz, Nature (London) **483**, 187 (2012).
[27] G. Paneru and H. K. Pak, Adv. Phys. X **5**, 1823880 (2020).
[28] D. Hennig, Phys. Rev. E **79**, 041114 (2009).
[29] K. Lichtner and S. H. L. Klapp, Europhys. Lett. **92**, 40007 (2010).
[30] H. Ando, K. Takehara, and M. U. Kobayashi, Phys. Rev. E **96**, 012148 (2017).
[31] S. Tarama, S. U. Egelhaaf, and H. Löwen, Phys. Rev. E **100**, 022609 (2019).
[32] R. A. Kopp and S. H. L. Klapp, Phys. Rev. E **107**, 024611 (2023).
[33] A. Curran, S. Tuohy, D. G. A. L. Aarts, M. J. Booth, T. Wilson, and R. P. A. Dullens, Optica **1**, 223 (2014).
[34] P. H. Jones, O. M. Maragó, and G. Volpe, *Optical Tweezers: Principles and Applications* (Cambridge University Press, Cambridge, UK, 2015).
[35] M. P. N. Juniper, A. V. Straube, R. Besseling, D. G. A. L. Aarts, and R. P. A. Dullens, Nat. Commun. **6**, 7187 (2015).
[36] J. R. Howse, R. A. L. Jones, A. J. Ryan, T. Gough, R. Vafabakhsh, and R. Golestanian, Phys. Rev. Lett. **99**, 048102 (2007).
[37] E. A. Codling, M. J. Plank, and S. Benhamou, J. R. Soc. Interface **5**, 813 (2008).
[38] S. Guillouzic, I. L'Heureux, and A. Longtin, Phys. Rev. E **59**, 3970 (1999).
[39] U. Küchler and B. Mensch, Stoch. and Stoch. Rep. **40**, 23 (1992).
[40] H. Wang and G. Oster, Europhys. Lett. **57**, 134 (2002).
[41] U. Seifert, Eur. Phys. J. B **64**, 423 (2008).
[42] K. Sekimoto, Prog. Theor. Phys **130**, 17 (1998).
[43] U. Seifert, Rep. Prog. Phys. **75**, 126001 (2012).
[44] T. Sagawa and M. Ueda, Phys. Rev. Lett. **104**, 090602 (2010).